

# Adaptive voltage controller based on extreme learning machine for DC-DC boost converter

Herlambang Setiadi<sup>1</sup>, Darmansyah<sup>2</sup>, Awan Uji Krismanto<sup>3</sup>, Sulthon Yusuf Abdillah<sup>4</sup>

<sup>1</sup>Electrical Engineering Study Program, School of Electrical Engineering, Faculty of Electrical Engineering, Telkom University, Bandung, Indonesia

<sup>2</sup>Department of Electrical Engineering, Faculty of Engineering, Universitas Lancang Kuning, Pekanbaru, Indonesia

<sup>3</sup>Department of Electrical Engineering, Faculty of Industrial Technology, Institut Teknologi Nasional, Malang, Indonesia

<sup>4</sup>Departemen of Engineering, Faculty of Advanced Technology and Multidiscipline, Universitas Airlangga, Surabaya, Indonesia

## Article Info

### Article history:

Received Dec 5, 2024

Revised Aug 11, 2025

Accepted Sep 1, 2025

### Keywords:

Adaptive voltage controller  
Clean energy technology  
Continus conduction mode  
DC-DC boost converter  
Extreme learning machine  
Proportional-integral controller

## ABSTRACT

This study presents an adaptive voltage controller for a DC-DC boost converter using the extreme learning machine (ELM) algorithm to address the limitations of conventional control techniques under varying load and reference voltage conditions. The ELM is implemented to predict the optimal parameters of a PI controller ( $K_p$  and  $K_i$ ), enabling real-time adaptability of the system. Simulation results in MATLAB/Simulink demonstrate that the proposed ELM-based proportional-integral controller (PI-ELM) outperforms both traditional PI controllers and those optimized using metaheuristic algorithms. Specifically, the controller achieved a maximum absolute error of only 0.0185 for  $K_p$  and 0.0294 for  $K_i$  across a range of operating conditions, with corresponding mean squared errors (MSE) of 0.01861 and 0.02798, respectively. These findings confirm the effectiveness of the ELM in enhancing the dynamic response and robustness of boost converter voltage regulation systems.

*This is an open access article under the [CC BY-SA](https://creativecommons.org/licenses/by-sa/4.0/) license.*



## Corresponding Author:

Herlambang Setiadi

Electrical Engineering Study Program, School of Electrical Engineering, Telkom University

St. Telekomunikasi No. 1, Terusan Buahbatu-Bojongsoang, Bandung, West Java 40257, Indonesia

Email: herlambangsetiadi@telkomuniversity.ac.id

## 1. INTRODUCTION

The advancement of power electronic devices has accelerated in line with the progression of the industry 4.0 era. Such devices play a crucial role in converting renewable energy—derived from sources like wind and photovoltaic (PV) systems—into both DC and AC electrical power [1], [2]. They are also widely implemented in energy storage technologies, including battery energy storage systems and superconducting magnetic energy storage units [3], [4]. Moreover, power electronic systems form an integral part of electric vehicle technologies [5]. Among the various types of power electronic converters, the DC–DC boost converter has gained prominence for its capability to modify and regulate DC voltage levels efficiently [6].

The use of DC–DC boost converters for maximum power point tracking (MPPT) in solar PV systems has been demonstrated in [7], where the converter effectively tracks the maximum power output of solar cells. Furthermore, incorporating a fuzzy logic–based control strategy for the boost converter significantly enhances PV power extraction efficiency. In the context of electric vehicles [8] reports that integrating a boost converter can substantially improve the performance of systems employing permanent magnet DC brushed motors. Similarly, the study in [9] highlights that a boost converter enables optimal energy harvesting from piezoelectric sources. The application of boost converters in fuel cell stacks is discussed in [10], while Turksoy *et al.* [11] presents their use in electric car battery charging systems. As

reflected in these works, the controller plays a pivotal role in determining the performance of a boost converter. Such controllers may be implemented using conventional design methods or enhanced through artificial intelligence (AI)-based approaches.

In recent years, the integration of AI into power systems has grown substantially. For instance, Wang *et al.* [12] reports the use of the differential evolution algorithm to determine the optimal placement of battery energy storage systems, enabling their deployment as charging stations with maximum efficiency. Ali *et al.* [13], a fuzzy logic controller is applied for MPPT, while Jagatheesan *et al.* [14] employs a flower pollination algorithm to design a proportional-integral-derivative (PID) controller for the secondary control of interconnected power systems. The firefly algorithm has been utilized in [15] for the design of a static synchronous series compensator. Additionally, Madhavi and Das [16] demonstrates the application of machine learning techniques for real-time monitoring of power system performance, allowing automatic acquisition of all critical parameters. Collectively, these studies indicate that AI-based approaches show strong potential for the design and optimization of various power system controllers.

This work presents a method for developing a boost converter voltage controller capable of adapting to varying operating conditions. The adaptability is achieved through the implementation of an extreme learning machine (ELM). The structure of the paper is as follows: section 2 outlines the theoretical background of the study, while section 3 describes the ELM and its application in designing the voltage controller. Section 4 presents the experimental results and corresponding analysis, and section 5 concludes the paper and discusses potential directions for future research.

## 2. METHOD

### 2.1. DC-DC step-up converter

The boost converter consists of a metal-oxide-semiconductor field-effect transistor (MOSFET), along with diodes, inductors, and capacitors. In a DC-DC boost converter, the output voltage is influenced by the operating time, and the output voltage is higher than the input voltage. The design focuses on the switching operation of the MOSFET within the boost converter. An illustration of the DC-DC boost converter is shown in Figure 1 [17]. For the optimal boost converter, a case study is provided to demonstrate the application of the transfer model under continuous conduction mode (CCM) operating conditions [18].

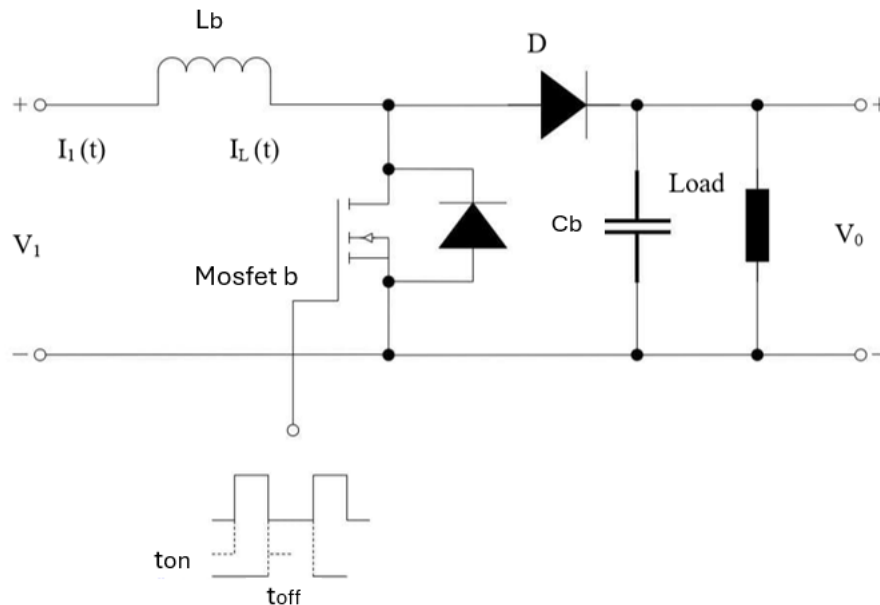


Figure 1. DC-DC boost converter electrical circuit

### 2.2. Continuous conduction mode operation of a DC-DC boost converter

As previously discussed, the bilinear form of any power converter can be derived in one of two ways: by listing all possible configurations and identifying common bilinear-based structures. Because this is a dc-dc converter example, the switching feature  $u$  may be changed in two ways to  $u=h_1=1-h_2$ . Status

variables include inductor current  $i_L$  and condenser voltage  $V_C$ . State space equation of DC-DC boost converter in (1) [17], [18].

$$u = 1; \begin{cases} i_L = E/L \\ \dot{V}_C = -V_C/RC \end{cases}, u = 0; \begin{cases} i_L = E/L - V_C/L \\ \dot{V}_C = i_L - V_C/RC \end{cases} \quad (1)$$

By introducing the switching function  $u$ , (1) can be expressed in a unified form, which is directly employed in simulations to represent the validation functions  $h_1$  and  $h_2$ . This formulation enables the derivation of the specified bilinear form [17], [18].

$$\begin{cases} \dot{i}_L = \frac{E}{L}u + \frac{E-V_C}{L}(1-u) \\ \dot{V}_C = -\frac{V_C}{RC}u + (\frac{i_L}{C} - \frac{V_C}{RC})(1-u) \end{cases} \quad (2)$$

From which one can derive:

$$\begin{cases} \dot{i}_L = -\frac{(1-u)V_C}{L} + E/L \\ \dot{V}_C = (1-u)(\frac{i_L}{C} - V_C/RC) \end{cases} \quad (3)$$

in (3) allows one to obtain the bilinear form:

$$\begin{pmatrix} \dot{i}_L \\ \dot{V}_C \end{pmatrix} = \underbrace{\begin{pmatrix} 0 & \frac{1}{L} \\ -\frac{1}{C} & 0 \end{pmatrix}}_B \begin{pmatrix} i_L \\ V_C \end{pmatrix} u + \begin{pmatrix} E/L \\ 0 \end{pmatrix} \quad (4)$$

with  $b = [0 \ 0]^T$ , (4) can describe in state variable form:

$$\dot{x} = A.x + B.x.u + d \quad (5)$$

The second approach begins by defining the state variables, where  $i_L$  and  $V_C$  serve as the state variables, like the previous method. In this case, the switching variables are the transistor voltage  $V_H$  and the diode current  $i_D$ , which can be expressed as functions of the state variables.

$$V_H = \begin{cases} 0 & \text{if H is on} \\ \dot{V}_C & \text{if H is off} \end{cases} \text{ and } \begin{cases} 0 & \text{if H is on} \\ i_L & \text{if H is off} \end{cases} \quad (6)$$

By applying the Kirchhoff voltage law to express  $di_L/dt$  and the current law for  $dV_C/dt$  Kirchhoff, as shown in Figure 2, we obtain the equations that describe the circuit compartment [17], [18]. It is:

$$\begin{cases} L \cdot \dot{i}_L = E - V_H \\ C \cdot \dot{V}_C = i_D - \frac{V_C}{R} \end{cases} \quad (7)$$

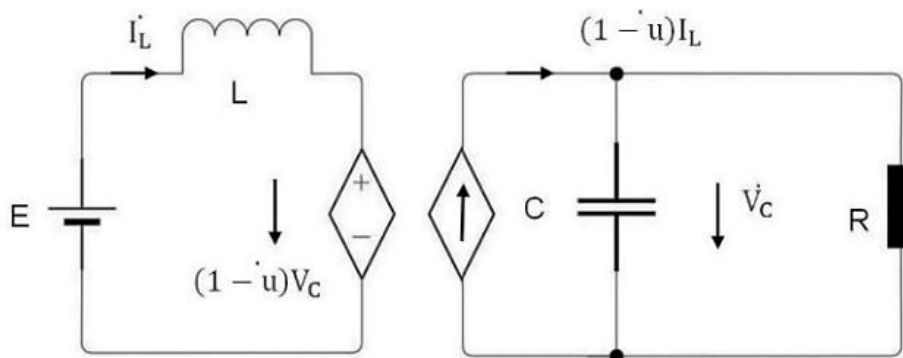


Figure 2. Equivalent circuit of a DC-DC boost converter operating in CCM

The transferred variable must also be represented as a function of an appropriately defined switching function. The following switching function is introduced:

$$u = \begin{cases} 1 & \text{if H is on} \\ 0 & \text{if H is off} \end{cases} \quad (8)$$

$$\begin{cases} V_H = V_C(1 - u) \\ i_D = i_L(1 - u) \end{cases} \quad (9)$$

By substituting (9) into (7), one obtains:

$$\begin{cases} \dot{i}_L = -\frac{(1-u)V_C}{L} + E/L \\ \dot{V}_C = (1-u)i_L/C - \frac{V_C}{RC} \end{cases} \quad (10)$$

The bilinear representation associated with the equation can be obtained using the same procedure applied to (2) and (3). As illustrated in Figure 2, the boost converter from (2) is modeled in CCM, independent of the specific approach employed to derive its bilinear form. In this model, the interaction between the input and output stages is expressed through two dependent sources, which emulate an ideal DC transformer whose turns ratio can be adjusted externally. To analyze the behavior of the system formulated in (1), a specialized simulation tool was created. The performance at the optimal boost point, implemented in Simulink®, is evaluated by observing the impact of varying the phase shift of the duty cycle [17], [18].

### 2.3. Pulse width modulation

To obtain different output voltages at the load, the duty cycle of the switching device is adjusted. The duty cycle is determined by comparing a DC reference signal with a sawtooth waveform of a specified frequency using a comparator, a method known as pulse width modulation (PWM). The maximum amplitude of the DC reference signal must be lower than the peak amplitude of the sawtooth waveform to ensure proper operation [19].

When the DC reference signal exceeds the sawtooth signal, the comparator output is  $V_{threshold}$  (ON). Conversely, when the DC reference signal is lower than the sawtooth signal, the comparator output is 0 (OFF). The duty cycle is generated based on the switching operation governed by the comparator. Its value depends on the duration for which the switch remains in the ON state. The duty cycle  $D$  can be calculated using the following expression, where  $D$  is the duty cycle (in %),  $t_{on}$  is the switch ON time, and  $T$  is the period of the sawtooth waveform [20].

$$D = \frac{t_{on}}{T} \times 100\% \quad (11)$$

### 2.4. Proportional–integral controller

In control systems, various methods can be employed to regulate system behavior, one of which is the proportional–integral (PI) controller. Each control strategy offers distinct advantages and limitations [21]. The primary advantage of a proportional controller is its ability to increase the system's rise time, enabling faster response. In contrast, integral control is effective in minimizing steady-state error. When proportional and integral control are combined, the resulting system exhibits both a faster rise time and reduced error compared to systems that do not employ such control strategies. This combined approach is known as a PI controller [22], [23]. The mathematical representation of the PI controller is described using (12).

$$u(t) = K_p e(t) + \frac{K_p}{T_i} \int_0^t e(t) dt \quad (12)$$

The output of a proportional controller is the result of multiplying an error value by the proportional gain. Because of its value limits, the proportional gain cannot be entered at random. If the proportional gain is set too high, the system may fail to reach a steady-state condition. Conversely, if the proportional gain is too low, the system's steady-state value will deviate from the desired set point. Therefore, proper tuning of the proportional gain is essential. The integral controller complements this by minimizing steady-state error through the integration of the error signal over time. Additionally, the integral action helps reduce the time required to eliminate offsets. The block diagram of the PI controller is presented in Figure 3 [22].

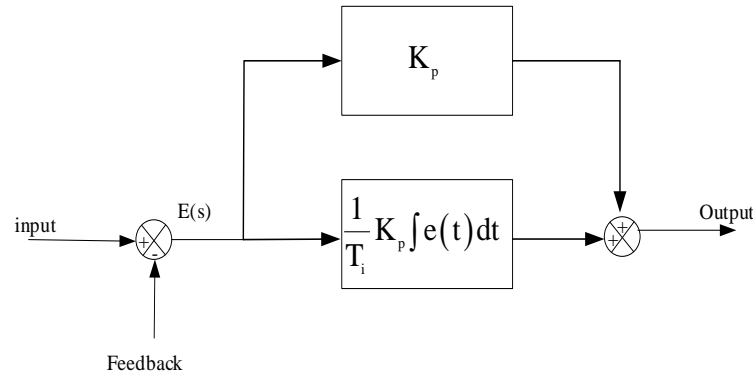


Figure 3. Block diagram of a PI controller

## 2.5. Extreme learning machine

The ELM has gained significant attention for solving a wide range of engineering and interdisciplinary problems. The ELM is based on a single hidden layer feedforward network (SLFN) architecture, developed to address the limitations of traditional SLFNs, particularly in learning efficiency. In ELM, the hidden layer parameters are randomly assigned and remain fixed, eliminating the need for iterative adjustment. This approach not only enables accurate generalization but also establishes the relationship between input and output data at a much faster rate compared to conventional learning algorithms such as the standard SLFN. Furthermore, the processing elements can be determined before the training data is collected. The slow learning rate of traditional SLFNs can be attributed to two primary factors [24]:

- The training procedure is carried out using a gradient based learning algorithm
- This learning approach determines parameters on the net by iteration

In the learning process, traditional gradient-based algorithms such as backpropagation, Levenberg–Marquardt, and similar methods, enquire manual computation of the parameters in an SLFN. Specifically, the input weights and hidden biases, which connect one layer to the next, must be iteratively adjusted. This results in slow learning speeds and a high likelihood of becoming trapped in local minimum. In contrast, the ELM overcomes these limitations. The output function of an ELM for a generalized SLFN can be expressed as in (13) [24].

$$y_L(x) = \sum_{i=1}^L \varphi_i \psi_i(x) = \psi(x)\varphi \quad (13)$$

Where  $\varphi = [\varphi_1, \dots, \varphi_L]^T$  between the buried layer of  $L$  nodes and the output node,  $T$  is a vector of output weight. The output vector of the hidden layer with regard to  $x$  is  $(x)=[i(x), \dots, L(x)]$ . The  $d$ -dimensional input data of ELM is translated to the  $L$ -dimensional hidden-layer feature space  $H$  by  $\psi(x)$ . The ELM method varies from traditional learning algorithms in that it aims to get not only the shortest error value but also the least norm of output weights at the same time, as indicated in (14):

$$\text{Minimize: } \|H\varphi - T\|^2, \|\varphi\| \quad (14)$$

Where  $H$  is the hidden-layer output matrix.

$$H = \begin{bmatrix} \psi(x_1) \\ \vdots \\ \psi(x_N) \end{bmatrix} = \begin{bmatrix} \psi_1(x_1) & \dots & \psi_L(x_1) \\ \vdots & \ddots & \vdots \\ \psi_1(x_N) & \dots & \psi_L(x_N) \end{bmatrix} \quad (15)$$

In (14) addresses the least-squares problem defined in (11) by applying the Karush–Kuhn–Tucker (KKT) optimality conditions [25].

$$\varphi = H^T \left( \frac{1}{\lambda_r} + HH^T \right)^{-1} T \quad (16)$$

Where  $I$ ,  $T$ , and  $\lambda_r$  are the identity matrix, target matrix, and regularization factor, respectively.  $T=[t_1, \dots, t_N]^T$ . The output of ELM may be derived by putting (16) into (13) as specified in (17) [25].

$$y(x) = \psi(x)H^T \left( \frac{1}{\lambda_r} + HH^T \right)^{-1} T \quad (17)$$

### 2.6. Design adaptive proportional–integral based on extreme learning machine

This section discusses the implementation of the ELM in a PI controller, enabling the controller to adapt to variations in voltage reference and load conditions. The training input data consist of the voltage reference and the load of the DC–DC boost converter, while the output corresponds to the predicted PI controller parameters  $K_p$  and  $K_i$ . The adaptive PI control process can be summarized in the following steps [26]:

- Step 1: use (17) to conduct the training procedure.
- Step 2: the accuracy of the predicted parameter is evaluated using the mean absolute error (MAE) calculated according to (18):

$$MSE = \sum_{i=1}^N \frac{(\tilde{y}_i - y_i)^2}{N} \quad (18)$$

Where  $\tilde{y}_i$  is predicted data yielded by the proposed learning algorithm, while  $y_i$  is actual data.  $N$  is the number of datasets utilized in the training phase.

- Step 3: display the results when the MSE value reaches its minimum; otherwise, repeat the process from step 1 until the lowest MSE is obtained [26].

## 3. RESULTS AND DISCUSSION

Three independent case studies were conducted in this part to investigate the performance of the suggested strategy (PI-ELM). The first case study is from ELM's training phase. In this case study, the ELM is evaluated against various inputs and outputs. After the PI has been trained using ELM, it is tested on the system. In the second case study, this testing is carried out. The proposed approach is evaluated against varied loads in the third case study. Three alternative possibilities are investigated in each case study. The first case involves a system with a traditional PI controller. The second case study is a system with an intelligent PI based on a metaheuristic algorithm.

This section depicts the training phase of an ELM-based PI controller. Table 1 shows the datasets utilized in this study for the training procedure. The PI controller datasheets shown in Table 1 are based on the tuning procedure utilizing the firefly algorithm. As input, the voltage references and load of the DC-DC boost converter are employed. Furthermore,  $K_p$  and  $K_i$  (PI parameters) represent the results of the training.

Table 1. Operating conditions and PI parameters

V (Volt)	R (Ohm)	$K_p$	$K_i$
20	96	0.8094	11.2176
21	97	0.9768	11.7743
22	98	0.9787	10.2227
23	99	0.9666	10.6261
24	100	1.0000	10.0000
25	101	1.0000	11.0879
26	102	0.9685	11.1635
27	103	0.9346	10.9627
28	104	0.9918	11.5189
29	105	0.8805	10.0854
30	106	0.9800	11.9800
31	107	1.0000	12.0000
32	108	0.8550	11.3176
33	109	0.9966	11.8843
34	110	0.9896	10.5554
35	111	0.8901	10.7771
36	112	0.9101	11.0666
37	113	1.0000	11.5534

Figures 4 and 5 show a comparison of real  $K_p$  and  $K_i$  parameters with  $K_p$  and  $K_i$  based on the ELM. The pattern of the graph shows that ELM can anticipate the values of  $K_p$  and  $K_i$  optimally. Tables 2 and 3 provide the detailed characteristics corresponding to Figures 4 and 5. From Table 2, it can be observed that the proportional gain ( $K_p$ ) exhibits a maximum error of 0.0185 and a minimum error of 0.0171, with a mean squared error (MSE) of 0.01861. For the integral gain ( $K_i$ ), the maximum and minimum errors are 0.0294 and 0.0280, respectively, with the minimum value calculated as 0.027983. These results indicate that the

overall error values are relatively low. Consequently, the training results demonstrate that the ELM is capable of accurately reproducing the actual PI controller parameters. Furthermore, the use of ELM enables the PI controller to adapt effectively to variations in both the converter's reference input and load conditions.

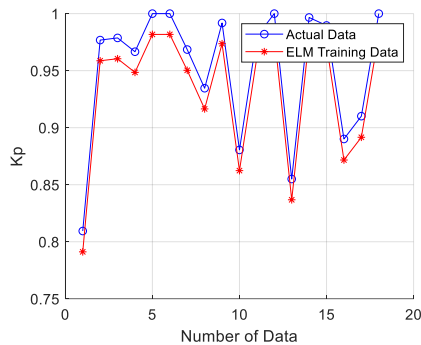


Figure 4. Kp trained parameter

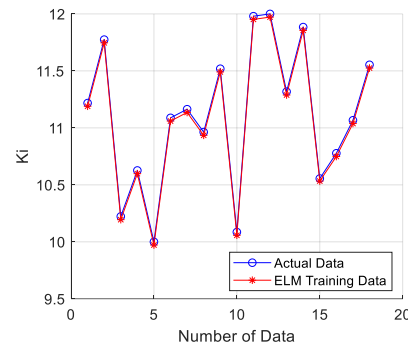


Figure 5. Ki trained parameter

Table 2. Comprehensive details of the system depicted in Figure 4

Actual Kp	ELM Kp	Error
0.8094	0.7912	0.0182
0.9768	0.9587	0.0181
0.9787	0.9605	0.0182
0.9666	0.9485	0.0181
1.0000	0.9818	0.0182
1.0000	0.9818	0.0182
0.9685	0.9503	0.0182
0.9346	0.9165	0.0181
0.9918	0.9736	0.0182
0.8805	0.8624	0.0181
0.9800	0.9618	0.0182
1.0000	0.9819	0.0181
0.8550	0.8368	0.0182
0.9966	0.9784	0.0182
0.9896	0.9725	0.0171
0.8901	0.8716	0.0185
0.9101	0.8916	0.0185
1.0000	0.9815	0.0185

Table 3. Comprehensive details of the system depicted in Figure 5

Actual Kp	ELM Kp	Error
11.2176	11.1894	0.0282
11.7743	11.7463	0.0280
10.2227	10.1945	0.0282
10.6261	10.5981	0.0280
10.0000	9.9718	0.0282
11.0879	11.0587	0.0282
11.1635	11.1353	0.0282
10.9627	10.9346	0.0281
11.5189	11.4908	0.0281
10.0854	10.0573	0.0281
11.9800	11.9517	0.0283
12.0000	11.9720	0.0280
11.3176	11.2882	0.0294
11.8843	11.8553	0.0290
10.5554	10.5334	0.0220
10.7771	10.7486	0.0285
11.0666	11.0380	0.0286
11.5534	11.5248	0.0286

To demonstrate the effectiveness of using the ELM algorithm, a comparative analysis was conducted against existing optimization techniques in terms of computational speed. Specifically, Table 4 presents a performance comparison among particle swarm optimization (PSO), the firefly algorithm, and ELM for determining the optimal parameters of a DC-DC PI controller. From the results shown in the table, it is evident that the ELM algorithm significantly outperforms both PSO and the firefly algorithm. ELM not only achieves faster convergence but also exhibits superior computational efficiency, making it a more suitable and effective approach for identifying the optimal control parameters in DC-DC converter systems.

Table 4. Execution time comparison

Index	Execution time (sec)
PSO	120
Firefly	140
ELM	0.003

#### 4. CONCLUSION

This study introduces an adaptive voltage control strategy for a DC-DC boost converter, employing an ELM to dynamically adjust the parameters of a PI controller. Simulation outcomes show that the ELM-based approach can accurately estimate the PI gains ( $K_p$  and  $K_i$ ) with minimal prediction error, ensuring high performance across a range of voltage references and load conditions. The maximum errors

recorded for  $Kp$  and  $Ki$  were 0.0185 and 0.0294, respectively, demonstrating the strong approximation capability of the ELM. Compared to conventional and metaheuristic-based controllers, the proposed system exhibited superior adaptability and robustness. These findings highlight the promise of ELM for real-time control in power electronic systems. Future research will focus on extending the method to MPPT in PV systems and in solar-powered electric vehicles.

## FUNDING INFORMATION

There is no contract or research number associated with this funding, as Telkom University only supported the article processing charge (APC) and did not sponsor the research itself.

## AUTHOR CONTRIBUTIONS STATEMENT

This journal uses the Contributor Roles Taxonomy (CRediT) to recognize individual author contributions, reduce authorship disputes, and facilitate collaboration.

Name of Author	C	M	So	Va	Fo	I	R	D	O	E	Vi	Su	P	Fu
Herlambang Setiadi	✓	✓	✓	✓	✓	✓	✓	✓	✓	✓	✓			✓
Darmansyah		✓				✓		✓	✓	✓				
Awan Uji Krismanto	✓		✓	✓			✓			✓				
Sulthon Yusuf						✓			✓	✓	✓			
Abdillah														

C : **C**onceptualization

M : **M**ethodology

So : **S**oftware

Va : **V**alidation

Fo : **F**ormal analysis

I : **I**nvestigation

R : **R**esources

D : **D**ata Curation

O : Writing - **O**riginal Draft

E : Writing - Review & **E**diting

Vi : **V**isualization

Su : **S**upervision

P : **P**roject administration

Fu : **F**unding acquisition

## CONFLICT OF INTEREST STATEMENT

Authors state no conflict of interest.

## DATA AVAILABILITY

Data availability is not applicable to this paper as no new data were created or analyzed in this study.

## REFERENCES




- [1] S. Gurung, S. Naetiladdanon, and A. Sangswang, "Coordination of power-system stabilizers and battery energy-storage system controllers to improve probabilistic small-signal stability considering integration of renewable-energy resources," *Applied Sciences*, vol. 9, no. 6, p. 1109, 2019, doi: 10.3390/app9061109.
- [2] D. Infield and L. Freris, *Renewable energy in power systems*, John Wiley & Sons, 2020.
- [3] U. Akram and M. Khalid, "A Coordinated Frequency Regulation Framework Based on Hybrid Battery-Ultracapacitor Energy Storage Technologies," *IEEE Access*, vol. 6, pp. 7310–7320, 2018, doi: 10.1109/ACCESS.2017.2786283.
- [4] H. Zhang *et al.*, "Design and control of a new power conditioning system based on superconducting magnetic energy storage," *Journal of Energy Storage*, vol. 51, p. 104359, Jul. 2022, doi: 10.1016/j.est.2022.104359.
- [5] R. Hou, L. Lei, K. Jin, X. Lin, and L. Xiao, "Introducing electric vehicles? Impact of network effect on profits and social welfare," *Energy*, vol. 243, p. 123002, 2022, doi: 10.1016/j.energy.2021.123002.
- [6] K. Nebti and R. Lebied, "Fuzzy maximum power point tracking compared to sliding mode technique for photovoltaic systems based on DC-DC boost converter," *Electrical Engineering & Electromechanics*, vol. 1, pp. 67–73, 2021, doi: 10.20998/2074-272X.2021.1.10.
- [7] A. Rajavel and N. R. Prabha, "Fuzzy logic controller-based boost and buck-boost converter for maximum power point tracking in solar system," *Transactions of the Institute of Measurement and Control*, vol. 43, no. 4, pp. 945–957, 2021, doi: 10.1177/0142331220938211.
- [8] P. Mishra, A. Banerjee, M. Ghosh, and C. B. Baladhandautham, "Digital pulse width modulation sampling effect embodied steady-state time-domain modeling of a boost converter driven permanent magnet DC brushed motor," *International Transactions on Electrical Energy Systems*, vol. 31, no. 8, p. e12970, 2021, doi: 10.1002/2050-7038.12970.
- [9] M. Edla, Y. Y. Lim, D. Mikio, and R. V. Padilla, "A single-stage rectifier-less boost converter circuit for piezoelectric energy harvesting systems," *IEEE Transactions on Energy Conversion*, vol. 37, no. 1, pp. 505–514, Mar. 2022, doi: 10.1109/TEC.2021.3103879.






- [10] A. R. Saxena and D. Kumar, "Transformerless high-gain battery-integrated DC-DC boost converter for fuel-cell stacks: Design, analysis, and control," *International Transactions on Electrical Energy Systems*, vol. 31, no. 2, p. e12722, 2021, doi: 10.1002/2050-7038.12722.
- [11] O. Turkoş, U. Yilmaz, and A. Teke, "Efficient AC-DC power factor corrected boost converter design for battery charger in electric vehicles," *Energy*, vol. 221, p. 119765, 2021, doi: 10.1016/j.energy.2021.119765.
- [12] S. Wang, L. Yu, L. Wu, Y. Dong, and H. Wang, "An Improved Differential Evolution Algorithm for Optimal Location of Battery Swapping Stations Considering Multi-Type Electric Vehicle Scale Evolution," *IEEE Access*, vol. 7, pp. 73020–73035, 2019, doi: 10.1109/ACCESS.2019.2919507.
- [13] M. N. Ali, K. Mahmoud, M. Lehtonen, and M. M. F. Darwish, "Promising MPPT Methods Combining Metaheuristic, Fuzzy-Logic and ANN Techniques for Grid-Connected Photovoltaic," *Sensors*, vol. 21, no. 4, p. 1244, 2021, doi: 10.3390/s21041244.
- [14] K. Jagatheesan, B. Anand, and S. Samanta, "Flower Pollination Algorithm Tuned PID Controller for Multi-source Interconnected Multi-area Power System," *Applications of Flower Pollination Algorithm and its Variants*, p. 221, 2021, doi: 10.1007/978-981-33-6104-1\_10.
- [15] A. Naderipour, Z. Abdul-Malek, V. K. Ramachandaramurthy, M. R. Miveh, M. J. H. Moghaddam, and J. Guerrero, "Optimal SSSC-based power damping inter-area oscillations using firefly and harmony search algorithms," *Scientific Reports*, vol. 10, no. 1, pp. 1–11, 2020, doi: 10.1038/s41598-020-69123-7.
- [16] S. V. Madhavi and G. T. R. Das, "Variable structure control for an isolated boost converter used in fuel cell applications," *International Journal of Electrical and Computer Engineering*, vol. 9, no. 6, p. 4493, 2019, doi: 10.11591/ijece.v9i6.pp4493-4506.
- [17] P. Vivek, N. B. Muthuselvan, and J. Nanadhaagopal, "Modeling of Solar PV System for DC-DC Converter with improved voltage stability Using Hybrid-Optimization Techniques," in *International Conference for Phoenixes on Emerging Current Trends in Engineering and Management (PECTEAM 2018)*, Atlantis Press, 2018, pp. 187–192, doi: 10.2991/pecteam-18.2018.33.
- [18] H. Y. Ahmed, O. Abdel-Rahim, and Z. M. Ali, "New High-Gain Transformerless DC/DC Boost Converter System," *Electronics (Basel)*, vol. 11, no. 5, p. 734, 2022, doi: 10.3390/electronics11050734.
- [19] H. Tarzamni, F. Tahami, M. Fotuhi-Firuzabad, and F. Blaabjerg, "Improved Markov model for reliability assessment of isolated multiple-switch PWM DC-DC converters," *IEEE Access*, vol. 9, pp. 33666–33674, 2021, doi: 10.1109/ACCESS.2021.3060950.
- [20] S. H. Montazeri, J. Milimonfared, and M. R. Zolghadri, "Multidimensional Pulse Width Modulation for Cascaded Split-Source Inverter," *IEEE Transactions on Industrial Electronics*, vol. 70, no. 1, pp. 137–146, Jan. 2023, doi: 10.1109/TIE.2022.3150087.
- [21] A. Baciú and C. Lazar, "Iterative Feedback Tuning of Model-Free Intelligent PID Controllers," *Actuators*, vol. 12, no. 2, 2023, doi: 10.3390/act12020056.
- [22] D. Ertekin, K. Bulut, H. Tekin, and G. Moschopoulos, "A design for switched capacitor and single-switch DC–DC boost converter by a small signal-based PI controller," *International Journal of Circuit Theory and Applications*, vol. 50, no. 5, pp. 1620–1651, 2022, doi: 10.1002/cta.3213.
- [23] M. Jabari, S. Ekinci, D. Izci, M. Bajaj, V. Blazek, and L. Prokop, "Efficient pressure regulation in nonlinear shell-and-tube steam condensers via a Novel TDn (1+ PIDn) controller and DCSA algorithm," *Scientific Reports*, vol. 15, p. 2090, 2025, doi: 10.1038/s41598-025-86107-7.
- [24] B. Liu, G. Chen, H.-C. Lin, W. Zhang, and J. Liu, "Prediction of IGBT junction temperature using improved cuckoo search-based extreme learning machine," *Microelectronics Reliability*, vol. 124, p. 114267, 2021, doi: 10.1016/j.microrel.2021.114267.
- [25] P. Pi and D. Lima, "Gray level co-occurrence matrix and extreme learning machine for Covid-19 diagnosis," *International Journal of Cognitive Computing in Engineering*, vol. 2, pp. 93–103, 2021, doi: 10.1016/j.ijcce.2021.05.001.
- [26] H. Setiadi *et al.*, "An Extreme Learning Machine Based Adaptive VISMA for Stability Enhancement of Renewable Rich Power Systems," *Electronics*, vol. 11, no. 2, p. 247, 2022, doi: 10.3390/electronics11020247.

## BIOGRAPHIES OF AUTHORS






**Herlambang Setiadi**    is Assistant Professor at School of Electrical Engineering, Telkom University. He received a bachelor degree from Institut Teknologi Sepuluh Nopember (Surabaya, Indonesia) majors in Power system Engineering in 2014. Then, master degree from Liverpool John Moores University (Liverpool, United Kingdom), majors in Electrical Power and Control Engineering in 2015. Furthermore, he received a Doctoral degree from The University of Queensland. Before joining Telkom University, he was investigator at INECS TEC Portugal and Lead Renewable Energy Engineering at Synkrona Enjiniring Nusantara. His research interests power system dynamic and control, renewable energy integration, and metaheuristic algorithm. He can be contacted at email: herlambangsetiadi@telkomuniversity.ac.id.






**Darmansyah**    is Lecturer at Electrical Engineering Department Faculty of Engineering Universitas Lancang Kuning (Pekanbaru, Indonesia). He received a bachelor degree from Universitas Bung Hatta (Padang, Indonesia) majors in Power System Engineering in 1998. Then, master degree from Institut Sain dan Teknologi Nasional (Jakarta, Indonesia), majors in Power System Engineering in 2010. Furthermore, he received a Doctoral degree from Institut Teknologi Sepuluh Nopember (Surabaya, Indonesia) majors in Power System Engineering in 2022. His research interests power electronics and control, renewable energy integration, and electric machines. He can be contacted at email: darmansyah@unilak.ac.id.



**Awan Uji Krismanto**    was born in Malang, Indonesia. He completed his B.Sc. and M.Sc. in Electrical Engineering from Brawijaya University and Sepuluh Nopember Institute of Technology (ITS), Indonesia in 2004 and 2010 respectively. He served as a faculty member in the Department of Electrical Engineering National Institute of Technology (ITN) Malang, Indonesia from 2005. He received a Doctoral degree from The University of Queensland. His research interests include power electronics, distributed generation, microgrid, renewable energy integration, and stability in power system. He can be contacted at email: [awan\\_uji\\_krismanto@lecturer.itn.ac.id](mailto:awan_uji_krismanto@lecturer.itn.ac.id).



**Sulthon Yusuf Abdillah**    is an undergraduate student from Airlangga University, Surabaya, majoring in Electrical Engineering. He is actively in Energy and Instrumentation Research Community as a member of Public Relations Division. He can be contacted at email: [h.setiadi@ftmm.unair.ac.id](mailto:h.setiadi@ftmm.unair.ac.id).